The Influence of Boundary Layer Parameters on Interior Noise

Dan Palumbo*
NASA Langley Research Center, Hampton, VA 23681

Joana Rocha†
University of Victoria, Victoria, BC, V8W 2Y2

Predictions of the wall pressure in the turbulent boundary of an aerospace vehicle can differ substantially from measurement due to phenomena that are not well understood. Characterizing the phenomena will require additional testing at considerable cost. Before expending scarce resources, it is desired to quantify the effect of the uncertainty in wall pressure predictions and measurements on structural response and acoustic radiation. A sensitivity analysis is performed on four parameters of the Corcos cross spectrum model: power spectrum, streamwise and cross stream coherence lengths and Mach number. It is found that at lower frequencies where high power levels and long coherence lengths exist, the radiated sound power prediction has up to 7 dB of uncertainty in power spectrum levels with streamwise and cross stream coherence lengths contributing equally to the total.

I. Introduction

The prediction of the vibration response and related acoustic radiation from a panel in the sidewall of an aerospace vehicle depends, fundamentally, on the cross spectrum matrix of the wall pressure. In this work the source is considered to be the Turbulent Boundary Layer (TBL). Over the years, several empirical models of the TBL wall pressure spectra have been developed, as described in Refs. [1-3]. It is assumed in these models that the TBL power spectral density (PSD) can be expressed as a stationary and homogeneous function, with zero mean pressure gradient. It is well established that the TBL cross power spectral density can be expressed as a product of a reference PSD function and a correlation function, such as described in Refs. [4-9]. The correlation function is usually written in a separable form in the streamwise and spanwise direction, in which the streamwise and spanwise functions decay exponentially with distance. Though more complex models exist, the empirical models developed by Corcos[4,5] and Efimtsov[6] provide a basis for our understanding of TBL wall pressure behavior. The parameters on which the Corcos cross spectrum model depends are reference power spectrum, flow convective velocity and coherence length. The reference power spectrum and coherence length are predicted using Efimtsov's models which, in turn, depend on flight conditions.

The results of a recent flight test[10] indicated that the measured wall pressure varied over short distances, at some locations agreeing with predictions, at others substantially deviating from predictions. This kind of spatial variability has been observed before[11] and had been attributed to differences in the flushness of the sensors[12]. For this reason, pin-hole sensors were used in a recent flight test and produced very well behaved data, except for the spatial variation in power spectrum. The observed behavior can not be modeled because it is not adequately understood. However, it can be said, with some confidence, that the observed variations in pressure spectra are a common occurrence over the surface of an aerospace vehicle. The question then becomes, "Does the observed variability in wall pressure spectra adversely impact predicted panel response and related radiation?". To answer this question, the sensitivity of predicted radiated sound power to variation in TBL cross spectrum parameters is estimated.

* Senior Engineer, Structural Acoustics Branch, MS 463, member AIAA
† Post Doc, Dept. of Mech. Engineering, 3800 Finnerty Rd.

II. Uncertainty in TBL Model Parameters

To predict a panel's response to a pressure field in the frequency domain, it is necessary to specify the pressure field's cross spectrum matrix across the surface of the panel. The Corcos cross spectrum model[4,5] of the turbulent boundary layer is widely used and is the basis for the definition of the source pressure field.

$$\Phi_{tbl}(r_x, r_y, \omega) = \Phi_{ref}(\omega) e^{\frac{-|r_x|}{L_x}} e^{\frac{-|r_y|}{L_y}} e^{\frac{-i\omega r_x}{U_c}} \quad (1)$$

In Eq. 1, Φ_{tbl} is the cross spectrum at position (r_x, r_y) with respect to a reference location (0, 0). The reference power spectrum, Φ_{ref}, is assumed to be constant over the field under consideration. Coherence lengths, L_x and L_y determine the rate of decay in the correlation in the x (streamwise) and y (cross stream) directions. Efimtsov[6] provides models for Φ_{ref}, L_x and L_y. These models will be presented in detail in "Reference power spectrum, Φ_{ref}." on page 8. Here we will compare the models' predictions to measurements obtained during a flight test.

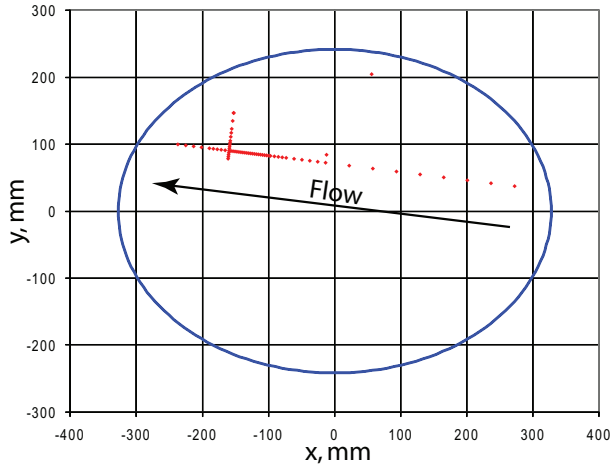

Fig. 1 Sketch of arrangement of sensor array in window blank.

A. The flight test

Gulfstream, Boeing and NASA conducted a cooperative flight test to acquire wall pressure data in an effort to validate and/or advance the models in use by the respective organizations[10]. The data were acquired from sensors mounted in a window blank installed in the forward window area of a G550 aircraft, Fig. 1. The sensor array was inclined at an angle of 5.5° to the fuselage axis to account for the angle of the streamline during cruise. There were a total of 43 sensors in the streamwise array spanning 47.7 cm and 15 sensors in the cross stream array spanning 8.1 cm. The sensors in the high density portions of the array were spaced 3 mm apart. Additional sensors spaced at 6 mm, 12 mm and 36 mm were added to increase the length of the arrays beyond the point of expected significant correlation. The pressure sensors were 1.6 mm in diameter with piezo-resistive elements operated in differential mode, vented to the cabin. The sensors were recessed behind a 0.254 mm stainless steel plate under pinholes which were 0.5 mm in diameter. The cavity above the sensors was 1.8 mm in depth and 1.45 mm in diameter. The usable bandwidth of the array is limited by the Helmholtz resonance of the cavity and pinhole. The Helmholtz resonance frequency for the cavity is approximately 15 kHz. The data were acquired at 204.8 kHz to maximize time resolution and for 60 seconds to provide adequate time for averaging.

Table 1 summarizes the flight test conditions where c is the speed of sound, U_∞ is the freestream velocity, x is the distance from the nose of the aircraft to the window blank, ν is the viscosity, Re is the Reynolds number, C_f is the coefficient of friction, u_τ is the friction velocity and δ is the boundary layer thickness. The three flight conditions will be referred to as Case 1, M=0.56; Case 2, M=0.7; and Case 3, M=0.8.

Table 1: Flight test conditions and flow parameters

Case	Mach Number	Altitude (ft)	c (m/s)	U_∞ (m/s)	x (m)	ν (m^2/s)	Re	C_f	u_τ (m/s)	δ (m)
1	**0.56**	**24000**	**311**	**174**	**6.7**	**2.7E-5**	**4.3E7**	**1.8E-3**	**5.2**	**7.6E-2**
2	**0.7**	**32000**	**301**	**210**	**6.7**	**3.4E-5**	**4.1E7**	**1.8E-3**	**6.3**	**7.7E-2**

Table 1: Flight test conditions and flow parameters

Case	Mach Number	Altitude (ft)	c (m/s)	U_∞ (m/s)	x (m)	ν (m^2/s)	Re	C_f	u_τ (m/s)	δ (m)
3	**0.8**	**48000**	**295**	**252**	**6.7**	**6.9E-5**	**2.5E7**	**2.0E-3**	**7.9**	**8.5E-2**

B. Comparing prediction to measurement

A typical PSD for a sensor along the streamwise array is compared to Efimtsov's prediction for the three flight conditions in Fig. 2a. As can be seen, the flight data is as much as 5 dB above the prediction around 1 kHz. The increased power in the flight data is accompanied by much longer coherence lengths as shown in Fig. 2b where the coherence lengths measured in the flight data are as much as 5 times those predicted.

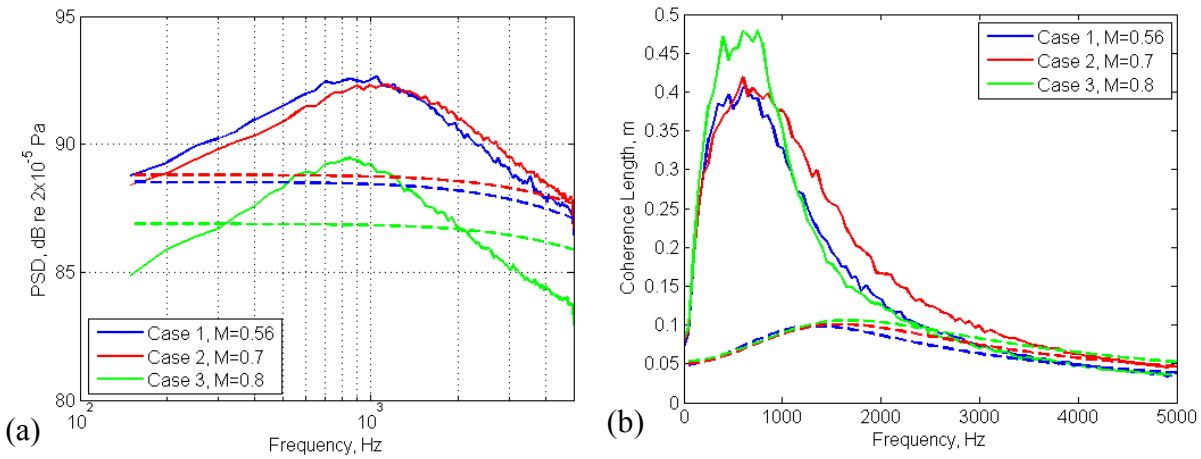

Fig. 2 Flight measurements (solid lines) compared to predictions (dashed lines) for power spectral density, (a) and coherence (b).

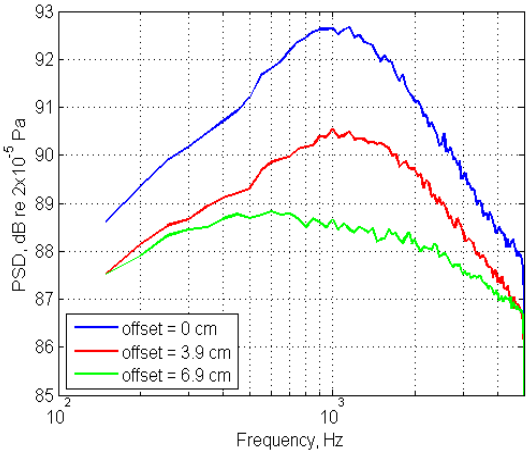

Fig. 3 Power spectral density taken at indicated offsets along the cross stream array for Case 2, M=0.7.

It can be argued that, if we were confident in the data (which were otherwise extraordinarily well behaved), then the models could be adapted to fit the data. However, as can be seen in the PSD measurements taken at different locations in the cross stream array (Fig. 3), the PSD is not spatially uniform. This behavior has been observed in another flight test[11] and had been explained by a lack of uniform sensor flushness with surface[12] which reasoning led to the pinhole array design used in the recent flight test. Any attempts to explain the observed variation would require additional testing either in-flight, in a wind tunnel or via numerical simulation. As all of the options are expensive, the need for additional testing must then be demonstrated. To this end, it is desired to understand the sensitivity of the radiated sound power prediction to the uncertainty in the model parameters.

III. Sensitivity Analysis

Given a system of multiple parameters, the system's sensitivity to a single parameter can be computed by the following

$$\Sigma_{p_i} = \frac{\varepsilon_{p_i}}{\varepsilon_T}\frac{\partial}{\partial p_i}F(p_1, p_2, \ldots), \tag{2}$$

where Σ_p is the sensitivity of the system to parameter p, ε_p is the uncertainty of parameter p, ε_T is the total system uncertainty and F is a function which relates the parameters to the system output. For our purposes, the output is radiated sound power, Π, with four input parameters: the reference auto power, Φ_{ref}, the Mach number, M, and the coherence lengths in the streamwise and cross stream directions, L_x and L_y. Their respective uncertainties are termed $\varepsilon_{\Phi ref}$, ε_M, ε_{Lx}, and ε_{Ly}. It is common, for example, in the case of measurements, to associate a parameter's uncertainty with the standard deviation and compute the total uncertainty as the square root of the sum of the squares of the parameters' uncertainties. In the data under consideration here, the uncertainty of interest does not stem from measurement, but, rather, the inaccuracy of the model's prediction. The uncertainty is in our understanding of the physical phenomena and the non-uniformity of the physical process over the spatial extent of our measurements. It is desired to compute the worst case effect of this variability on our predictions of radiated sound power. To accomplish this, the uncertainties are estimated as the maximum differences found between measurement and prediction, except for Mach number whose uncertainty is assumed to be 1%. Partial function, F_p, is found empirically by varying a single parameter over a range of values that include the parameter uncertainty. The partial derivative of this function is termed the sensitivity coefficient of the system to the parameter. The total system uncertainty can then be computed as the sum of the product of the parameters' uncertainty and their respective sensitivity coefficients,

$$\varepsilon_T = \varepsilon_{\Phi_{ref}}\left|\frac{\partial F_{\Phi_{ref}}}{\partial \Phi_{ref}}\right| + \varepsilon_M\left|\frac{\partial F_M}{\partial M}\right| + \varepsilon_{L_x}\left|\frac{\partial F_{L_x}}{\partial L_x}\right| + \varepsilon_{L_y}\left|\frac{\partial F_{L_y}}{\partial L_y}\right|. \tag{3}$$

Complete details can be found in Ref. 14.

IV. Source, Response and Radiation Models

The sensitivity analysis will be performed on a system consisting of a single panel excited on one side by a pressure field representing a turbulent boundary layer and radiating to the free field on the other. An analytical model for the coupled system of turbulent boundary source, panel sidewall vibration and interior cavity response has been developed by da Rocha[15]. The approach in this paper will be slightly different as the system contains only a single panel and radiates to free space. The coupled solutions developed by da Rocha[15] will be used to predict the panel response and this response will be used in a model based on Wallace's solution[16] to predict the radiated sound power, as derived in Rocha[14]. If H is the transfer function from boundary layer excitation to panel displacement, the cross spectrum matrix of the panel displacement, Φ_{ww}, can be written as

$$\Phi_{ww} = H'\Phi_{tbl}H^T \tag{4}$$

where H' is the conjugate and H^T is the transpose of H. Given a modal radiation matrix, R, derived from Wallace's farfield intensity predictions[16] and the panel velocity cross spectrum matrix, $\Phi_{vv} = -\omega^2\,\Phi_{ww}$, the radiated sound power can be written as

$$\Pi = \Phi_{vv}R. \tag{5}$$

The following sections provide some detail on the formulations of Φ_{tbl}, H and R. For complete details, refer to Refs. [14-16].

A. Turbulent boundary layer cross spectrum model

As mentioned earlier, the Corcos form for the cross spectrum in the boundary layer will be utilized, Eq. 1. In this study, the convection velocity, U_c, is assumed to be 70% of the free stream velocity. The remaining parameters are taken from Efimtsov's theory[6]. The coherence lengths are defined as follows,

$$L_x = \delta\left[\left(\frac{a_1 Sh}{U_c/u_\tau}\right)^2 + \frac{a_2^2}{Sh^2 + (a_2/a_3)^2}\right]^{-1/2}, \text{ and,} \tag{6}$$

$$L_y = \delta\left[\left(\frac{a_4 Sh}{U_c/u_\tau}\right)^2 + \frac{a_5^2}{Sh^2 + (a_5/a_6)^2}\right]^{-1/2}, \text{ for M<0.75, and,} \tag{7}$$

$$L_y = \delta\left[\left(\frac{a_4 Sh}{U_c/u_\tau}\right)^2 + a_7^2\right]^{-1/2}, \text{ for M>0.9.} \tag{8}$$

The Strouhal number and friction velocity are defined as, $Sh = \omega\delta/u_\tau$ and $u_\tau = U_\infty\sqrt{C_f/2}$ respectively. The boundary layer thickness, δ, and coefficient of friction, C_f are:

$$\delta = 0.37 x Re^{-1/5}\left[1 + \left(\frac{Re}{6.9\times 10^7}\right)^2\right]^{1/10}, \text{ and,} \tag{9}$$

$$C_f = 0.37(\log_{10} Re)^{-2.584} \tag{10}$$

where $Re = U_\infty \frac{x}{\nu}$ is the Reynolds number, x is the distance to the sensor and ν is the viscosity (see Table 1). The parameters a_1 - a_7 are, respectively, 0.1, 72.8, 1.54, 0.77, 548, 13.5 and 5.66. The cross stream coherence lengths for Case 3, M=0.8, are interpolated using Eq. 7 and Eq. 8.

The reference power spectrum, Φ_{ref}, is given as

$$\Phi_{ref} = 2\pi\alpha_1 u_t^3 \rho^2 \delta \frac{\beta_1}{(1 + 8\alpha_1^3 Sh^2)^{1/3} + \alpha_1\beta_1 Re_\tau\left(\frac{Sh}{Re_\tau}\right)^{10/3}}, \tag{11}$$

where $\alpha_1 = 0.01$ and

$$\beta_1 = \left[1 + \left(\frac{Re_{\tau 0}}{Re_\tau}\right)^3\right]^{1/3}; \quad Re_{\tau 0} = \frac{\delta u_t}{\nu} \text{ and } Re_t = \frac{\delta u_\tau}{\nu_w} \tag{12}$$

$$\nu_w = \nu\left(\frac{T_w}{T}\right)^{r+1} ; \; T_w = T\left(1 + r\frac{k-1}{2}M^2\right) \tag{13}$$

with $r = 0.89$ and $k = 1.4$. Ambient temperature, T, is in Kelvin and the w subscript indicates these are measured at the wall.

Table 2: Panel Physical Properties

Variable	Description, units	Value
a	**length, m**	**0.414**
b	**width, m**	**0.314**
h	**thickness, m**	**0.001**
E	**Elasticity modulus, Pa**	**7.24 x 10^{10}**
ν_p	**Poisson ratio**	**0.33**
ρ	**Density, kg m^{-3}**	**2800**
ζ_p	**damping ratio**	**0.01**
N_x	**longitudinal tension, N m^{-1}**	**29300**
N_y	**lateral tension, N m^{-1}**	**62100**
c_a	**internal sound speed, m s^{-1}**	**340**
ρ_a	**internal density of air, kg m^{-3}**	**1.42**

B. Panel response model

The panel is assumed to be simply supported so that its displacement can be described in terms of a series of modes.

$$w_{mn}(x,y) = A_{mn}\sin\left(\frac{m\pi x}{a}\right)\sin\left(\frac{n\pi y}{b}\right), \tag{14}$$

In Eq. 14, w_{mn} is the panel displacement for mode (m,n), x and y are confined to panel dimensions a and b, and A_{mn} is the modal amplitude. The panel is assumed to be tensioned (under pressure) so that the modal frequencies are defined as

$$\omega_{mn} = \sqrt{\frac{1}{\rho h}[D(k_x^2 + k_y^2)^2 + N_x k_x^2 + N_y k_y^2]}, \tag{15}$$

where ρ is the panel density, h is the panel thickness, $D = \frac{Eh^3}{12(1+\nu_p)}$ is the panel stiffness, $k_x = m\pi/a$, $k_y = n\pi/b$ and N_x and N_y are the panel tension in the x and y directions respectively. The panel is assumed to be made of aluminum. Quantities for the material properties and panel dimensions are given in Table 2. Details of the coupled solution are given in da Rocha[15]. Convergence of the solution in the band from 200 Hz to 5 kHz was achieved using modes up to m=19 and n=14.

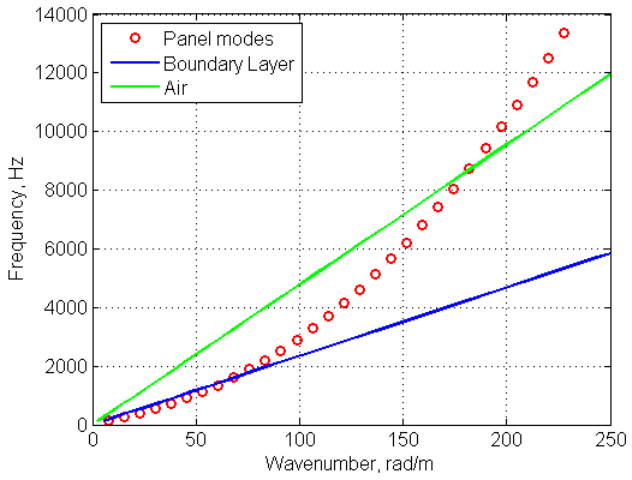

Fig. 4 Frequency dependence on wavenumber for panel modes, boundary layer and air.

When the wavenumber of the pressure fluctuations in the boundary layer is equal to the wavenumber of the bending wave in the panel, the boundary layer can efficiently transfer energy into the panel. The frequency at which this occurs is called the hydrodynamic coincidence frequency and occurs for the 9th mode around 68 rad/m and 1600 Hz at M=0.7, see Fig. 4. All modes near coincidence will have high coupling efficiencies. This occurs in the frequency range from very low frequencies to just above coincidence. Further above coincidence, the modal wavenumbers move away from the convection wavenumbers and have increasingly poorer coupling factors. As will be discussed in "Sensitivity Coefficients" on page 8, the sensitivity of radiated sound power to some boundary layer parameters will depend on frequency and the degree of coincidence at that frequency.

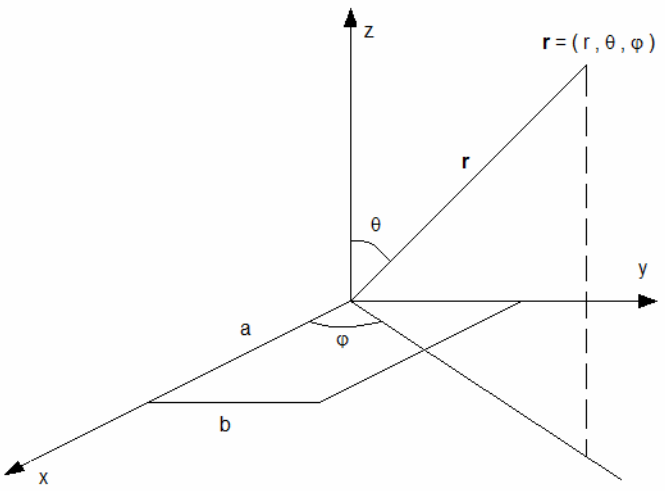

Fig. 5 Coordinate system for panel radiation.

C. Radiation model

Given a simply supported panel radiating into free space as shown in Fig. 5, Wallace[16] derives an expression for the farfield acoustic intensity of an infinitely baffled panel mode as

$$I_{mn} = 2\rho_0 c_0 \left(\frac{v_{mn} k_0 ab}{\pi^3 rmn}\right)^2 \Theta_{mn}, \tag{16}$$

where ρ_0 ,c_0 and k_0 are the density, speed of sound and wavenumber of air, respectively, v_{mn} is the panel velocity mode shape and Θ is defined as

$$\Theta_{mn} = \left[\frac{\begin{matrix}\cos\left(\frac{\alpha}{2}\right) & \cos\left(\frac{\beta}{2}\right)\\ \sin\left(\frac{\alpha}{2}\right) & \sin\left(\frac{\beta}{2}\right)\end{matrix}}{[(\alpha/m\pi)^2 - 1][(\beta/n\pi)^2 - 1]}\right]^2, \tag{17}$$

where $\alpha = k_0 a \sin\theta\cos\varphi$ and $\beta = k_0 b \sin\theta\sin\varphi$. In Θ_{mn}, the cosine functions are used with arguments $\left(\frac{\alpha}{2}\right)$ and $\left(\frac{\beta}{2}\right)$ for m,n odd, respectively, and the sine functions used for m,n even.

Taking advantage of symmetry in the squared velocity, the acoustic intensity in Eq. 16 can be integrated over a quarter space to yield the radiated sound power for a particular mode.

$$\Pi_{mn} = 8\frac{\rho_0}{c_0}\left(\frac{v_{mn}\omega ab}{\pi^3 mn}\right)^2 \int_0^{\frac{\pi}{2}}\int_0^{\frac{\pi}{2}} \Theta_{mn}\sin\theta\, d\theta\, d\varphi \tag{18}$$

Constructing a panel modal velocity vector, **V**, from the v_{mn}, a radiated sound power matrix can be computed as

$$\boldsymbol{\Pi}(\omega) = \boldsymbol{V}^T \boldsymbol{R}(\omega)\boldsymbol{V}, \tag{19}$$

where radiation matrix, **R**(ω) is defined as

$$\boldsymbol{R}(\omega) = 8\frac{\rho_0}{c_0}\left(\frac{\omega ab}{\pi^3 mn}\right)^2 \int_0^{\frac{\pi}{2}}\int_0^{\frac{\pi}{2}} \Theta_{mn}\sin\theta\, d\theta\, d\varphi\,. \tag{20}$$

Finally, the radiated sound power matrix can be written in terms of the panel velocity power, Φ_{vv} ,

$$\boldsymbol{\Pi}(\omega) = \boldsymbol{\Phi}_{vv}\boldsymbol{R}(\omega) \tag{21}$$

The concept of wavenumber coincidence is as relevant to the panel-acoustic radiation interface as it is to the panel-boundary layer interface. Acoustic coincidence is seen to occur around 9 kHz and 180 rad/m in Fig. 4. The physics governing radiation from a flat plat require the panel wavenumbers to be less than those in air. This occurs for frequencies above the acoustic coincidence. Thus, at M = 0.7 and for the range of frequencies between 2 kHz (the hydrodynamic coincidence frequency) and 8 kHz, the panel is a very poor converter of energy from boundary layer flow to acoustic radiation. If the panel material were lighter and stiffer, the panel modes in Fig. 4 would shift upwards towards higher frequencies with the result that both coincidence frequencies would move lower in frequency. The frequency band of efficient radiation then becomes wider while the band of efficient boundary layer energy absorption becomes narrower. As the Mach number increases and the slope of the convection wavenumber line approaches that of air's, the frequency band of efficient boundary layer energy absorption will get wider (hydrodynamic coincidence frequency will increase). Reduced mass, increased stiffness and increased speeds, will constructively combine to create a very efficient system for the conversion of boundary layer energy to acoustic radiation.

V. Sensitivity Coefficients

The radiated sound power's sensitivity to parameters of the Corcos cross spectrum model is dependent on the sensitivity coefficients, $\partial F_i / \partial p_i$, see Eq. 2. The sensitivity coefficients are taken from an empirical model of an individual parameter's influence on the radiated sound power, F_p. The empirical model is fit to points which result from the prediction of the total radiated sound power over a range of the parameter dictated by the difference between the measurements and predictions. The simplest relationship is presented first, Φ_{ref} , followed by M, L_y and finishing with the most complex case, L_{x}.

A. Reference power spectrum, Φ_{ref}.

The radiated sound power is directly proportional to the panel vibration response, Eq. 5, which, in turn, is directly proportional to the boundary layer cross spectrum, Eq. 4. Inspection of the Corcos cross spectrum model, Eq. 1, reveals that the boundary layer cross spectrum is also directly proportional to the reference power spectrum which leads one to the conclusion that the radiated sound power is directly proportional to the reference power spectrum. The relationship has been verified analytically, but is trivial. A 1 dB increase in boundary layer power produces a 1 dB increase in radiated sound power.

$$\Pi(\Phi_{ref} + x[dB]) = \Pi(\Phi_{ref}[dB]) + x[dB]\,. \tag{22}$$

The sensitivity coefficient of radiated sound power to reference power spectrum is then 1 dB/dB. The sensitivity in linear units can be found by writing,

$$\Pi(\Phi_{ref})[dB] = 10\log_{10}\left(\frac{\Phi_{ref}[Pa^2/Hz]}{4\times 10^{-10}}\right)[dB], \tag{23}$$

so that the sensitivity becomes 4.34 dB/(Pa^2/Hz).

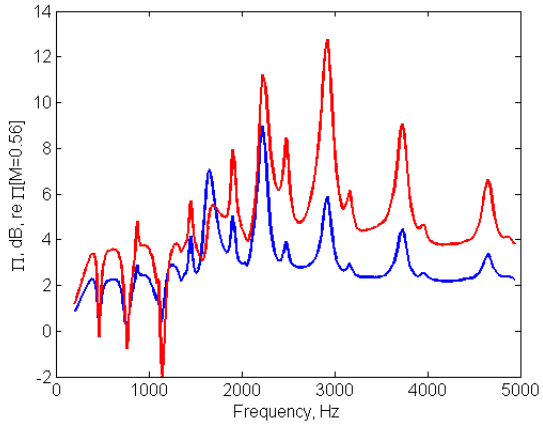

Fig. 6 Radiated sound power for M=0.7, blue and M=0.8, red, with respect to M=0.56.

B. Mach number, M

Keeping Φ_{ref}(M=0.7), L_x=0.2 m and L_y=0.02 m constant, the radiated sound power for M=0.56, 0.7 and 0.8 is computed. The results are plotted relative to the M=0.56 case in Fig. 6. It is apparent that the relationship depends on whether the frequency is below or above hydrodynamic coincidence (1600 Hz). The functions relating radiated sound power to changes to Mach number are, for frequencies below coincidence,

$$\Pi(M) = 9.9M - 4.4 + \Pi(\mathrm{M}=0.56), \tag{24}$$

and,

$$\Pi(M) = 27.4M - 16.4 + \Pi(\mathrm{M}=0.56), \tag{25}$$

above coincidence with Π(M=0.56) = -130.6 dB (re. 1 watt) below coincidence and -180.5 dB above coincidence. The sensitivity coefficient of the radiated sound power to Mach number is then 9.9 dB below coincidence and 27.4 dB above coincidence.

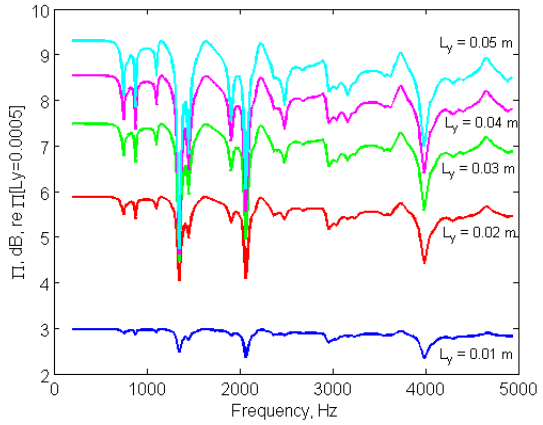

Fig. 7 Radiated sound power for L_y = 0.01 m, 0.02 m, 0.03 m, 0.04 m and 0.05 m with respect to L_y = 0.005 m

C. Cross stream coherence length, L_y

The radiated sound power plots for L_y = 0.01 m, 0.02 m, 0.03 m, 0.04 m and 0.05 m relative to L_y = 0.005 with Φ_{ref}(M=0.7), L_x=0.2 and M=0.7 constant are shown in Fig. 7. As might be expected, the relationship shows no dependence on the coincidence frequency. Also apparent is the expected behavior where radiated sound power increases with coherence length. The radiated sound power dependence on L_y is found to be

$$\Pi(L_y) = 3.67\ln(L_y) + 19.9 + \Pi(L_y{=}0.005), \tag{26}$$

with Π(L_y=0.005) = -142.5 dB. The sensitivity coefficient of the radiated sound power to the cross stream coherence length is then $3.67/L_y$ dB/m.

D. Streamwise coherence length, L_x

The radiated sound power's dependence on streamwise coherence length keeping Φ_{ref}(M=0.7), L_y=0.02 and M=0.7 constant is shown in Fig. 8. It is immediately apparent in Fig. 8(a) that a counterintuitive relationship exists between radiated sound power and the streamwise coherence length where radiated sound power decreases with coherence length. This is especially true above coincidence, but not true over the entire range of frequencies. A close up of the behavior around coincidence is shown in Fig. 8(b) where it can be seen that the radiated sound power is proportional to streamwise coherence at a mode near coincidence and inversely proportional at a mode above coincidence. This behavior is a result of the fluid's interaction with the panel and will be explained more completely in the next section. The empirical relationship is derived at the modal frequencies because this is where this behavior is most apparent. The functional relationship between radiated sound power and streamwise coherence below coincidence is

$$\Pi(L_x) = 3.73\ln(L_x) + 1.23 + \Pi(L_x{=}0.05) \tag{27}$$

and

$$\Pi(L_x) = -3.69\ln(L_x) - 11.1 + \Pi(L_x{=}0.05) \tag{28}$$

above coincidence with $\Pi(L_x{=}0.05)$ = -111 dB in Eq. 27 and -163 dB in Eq. 28. The sensitivity coefficient is $3.73/L_x$ dB/m below coincidence and $-3.69/L_x$ dB/m above.

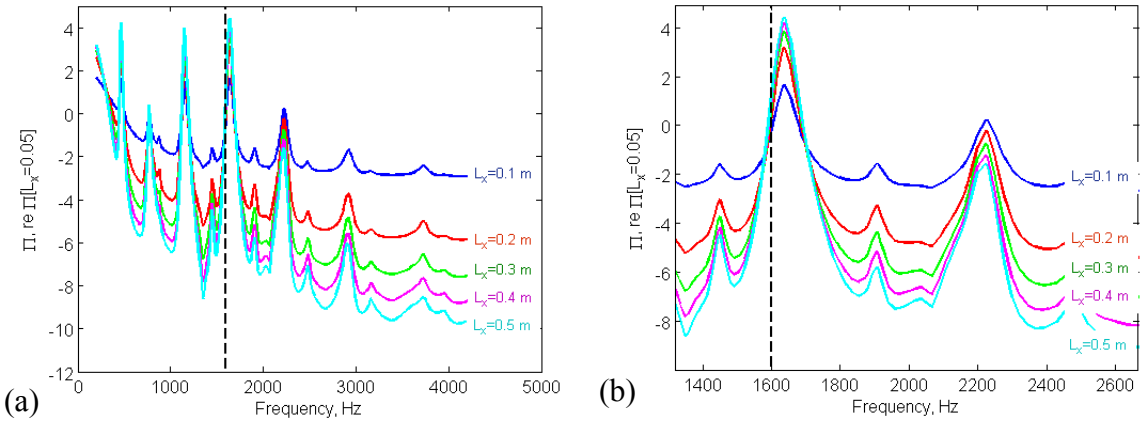

Fig. 8 Radiated sound power for L_x = 0.1 m, 0.2 m, 0.3 m, 0.4, m and 0.5 m with respect to L_x = 0.05 m. Full frequency range, (a), zoom to coincidence frequency, (b). The dashed line marks the hydrodynamic coincidence frequency.

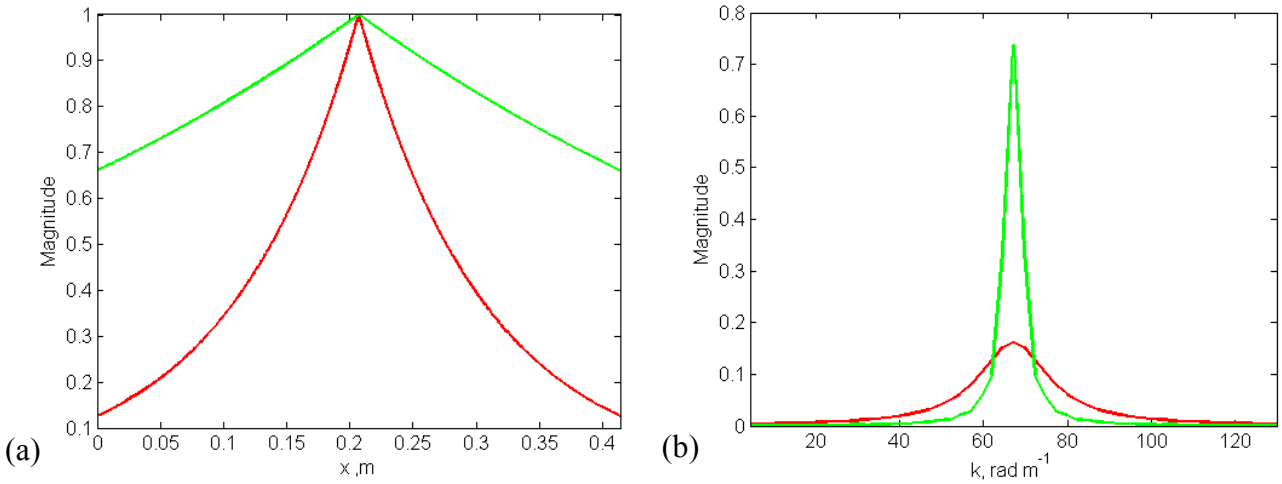

Fig. 9 Coherence decay curves, (a) and respective wavenumber spectra, (b), for coherence lengths of 0.1 m, red, and 0.5m green at M=0.7.

1.Streamwise Coherence Length and Modal Coupling

The dependence of the radiated sound power on the cross stream coherence behaved as one might expect, the radiated sound power increased with coherence length. As the cross stream coherence length increases, the surface area over which the coherent energy in the flow acts on the panel increases proportionally. The coupling of the streamwise coherence, on the other hand, is dependent on the fluid convection velocity and its relationship to the panel's dynamics. As explained in "Panel

response model" on page 6, the transfer of energy from the boundary layer to the panel depends on the wavenumber content of the boundary layer and how well the wave numbers in the flow match the bending wavenumbers in the panel. As seen in Fig. 4, the boundary layer and panel modal wavenumbers are in coincidence for M=0.7 and panel longitudinal mode number, m=9 which occurs near 1600 Hz. This case will be explored in more detail.

The coherent power in the boundary layer cross spectrum is enveloped by an exponential curve defined by the coherence length, Eq. 6. Fig. 9(a) illustrates the envelope shapes for L_x=0.1 m and L_x=0.5 m, the extremes of prediction and observation. When transformed to wavenumber space, the energy represented by the coherence curves will be centered at a wavenumber governed by the frequency and convection velocity (ω/U_c), but distributed around this wavenumber according to the shape of the coherence curve.

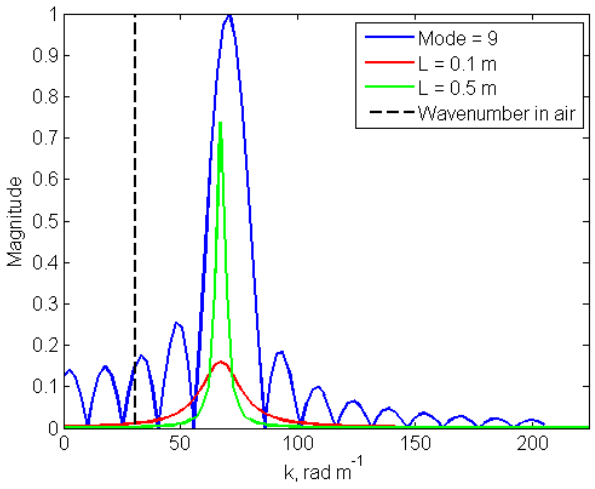

Fig. 10 Wavenumber spectra of mode 9, blue, L_x=0.1, red, L_x=0.5, green, and wavenumber in air, dashed line.

Fig. 9(b) is the wavenumber spectra of the two coherence curves. Note that the slowly decaying coherence curve for L_x=0.5 m becomes a narrow, sharply pointed, curve in wavenumber space while the faster decaying coherence curve for L_x=0.1 m becomes a broad curve in wavenumber space. The longer coherence length curve concentrates more energy around the fundamental wavenumber of the flow while the shorter coherence length spreads the energy out over wavenumber space. This concept is central to understanding the behavior seen in Fig. 8.

The wavenumber spectra of the long and short coherence curves are displayed along with the wavenumber spectra for mode 9 in Fig. 10. Both the long and short coherence spectra are in coincidence with the mode, but the long coherence spectra has most of its energy concentrated in the root lobe of the mode. The long coherence length energy will, therefore, couple its energy most efficiently into this mode. Contrast this situation with what occurs for mode 15 at 3700 Hz, Fig. 11(b). In this case the flow's wavenumber is not coincident with the mode's root lobe. The energy with short coherence lengths (red curve) has greater energy available in the lower wavenumbers to couple efficiently into mode 15. For completeness, mode 5 is shown in Fig. 11(a). In this case the energy in the flow is still coincident with the mode's root lobe enabling the energy in longer coherence lengths to couple more efficiently.

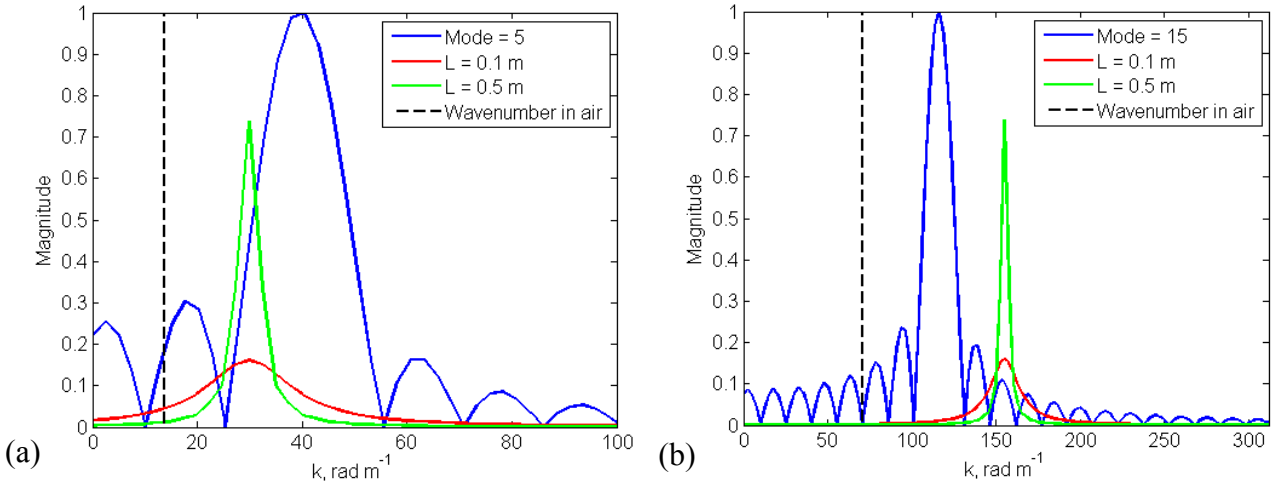

Fig. 11 Wavenumber spectra for mode 5 at 713 Hz, (a) and mode 15 at 3700 Hz, (b).

At frequencies where the mode is weak or nonexistent, the broader spread of the short coherence length energy into the lower wavenumbers has another effect. The wavenumber in air is noted in Fig. 11 by a dashed line. All energy in

wavenumbers at or below the wavenumber in air will radiate efficiently. By virtue of its broader tail, short coherence length energy will contain supersonic wavenumbers and therefore radiate more efficiently. This effect causes the gradual increase in radiation at lower frequencies observable in Fig. 8. If the frequency bandwidth of the analysis were wider, an increase in non-resonant radiation would be seen as the panel approached acoustic coincidence.

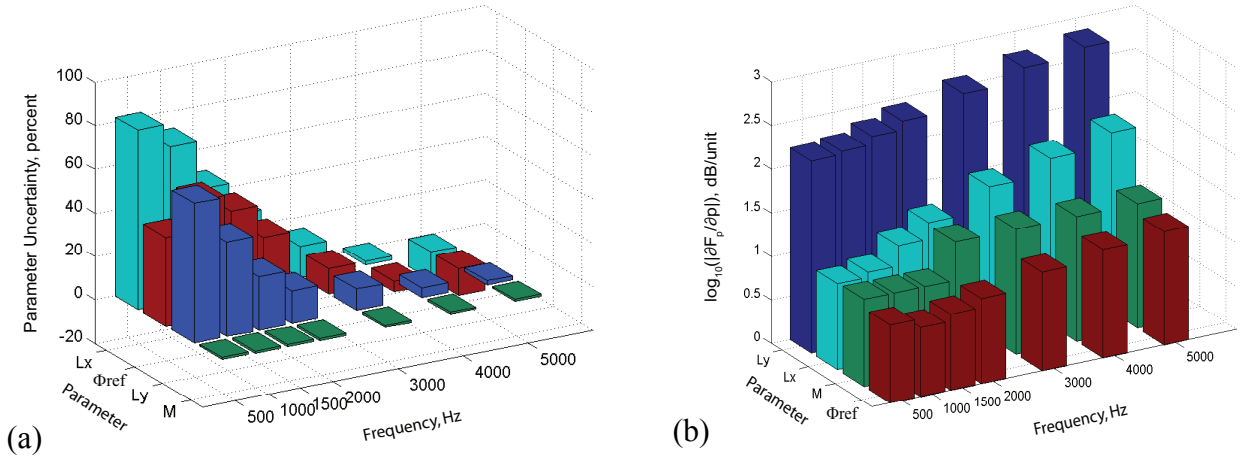

Fig. 12 Parameter uncertainty, ε_p, percent of measured value, (a) and sensitivity coefficient, $\partial F_p / \partial p$, (b).

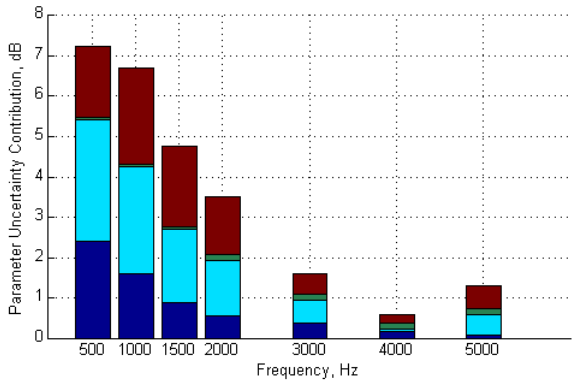

Fig. 13 Total uncertainty in terms of parameter contributions: L_y, L_x, M and Φ_{ref}

VI. Results

The L_x, L_y and Φ_{ref} parameter uncertainties are computed as the difference between the measured and predicted values and are displayed in Fig. 12(a) as percentages with respect to the measured value. As can be seen, these uncertainties are very high in the range 500 Hz to 2000 Hz. The uncertainty for Mach number, M, is assumed to be 1%.

The base 10 logarithm of the absolute value of the sensitivity coefficients are displayed in Fig. 12(b). The radiated sound power is very sensitive to the cross stream coherence with sensitivity coefficients over 100 dB/m. The streamwise coherence length sensitivity coefficients range from 10 dB/m in the lower frequencies to 100 dB/m at the higher frequencies. The elevated sensitivities of the coherence lengths at high frequencies are offset by their reduced uncertainties at those frequencies. The Mach number coefficients vary from 10 dB to 30 dB. The reference power spectrum has a sensitivity between 10 and 40 dB/(Pa^2/Hz) throughout the frequency range.

The total system uncertainty and its constituent parameter uncertainties are shown in Fig. 13. The total uncertainty is over 7 dB at the lower frequencies and is composed of nearly equal amounts of uncertainty in the coherence lengths and the reference power spectrum. At the higher frequencies, the total uncertainty is approximately 1 dB. The Mach number has comparatively no influence at low frequencies and very little at the higher frequencies.

VII. Conclusion

The prediction of radiated sound power stimulated by the boundary layer acting on a typical airframe panel was found to have a worst case uncertainty of over 7 dB based on the available data. All the uncertainty can be attributed to the power spectrum and coherence length models' underprediction of the measured values. While it is possible to adapt the models to match specific measured data, the physics underpinning the observed spatial variations in boundary layer behavior are not well understood, making it difficult to construct a model that will predict the behavior over the vehicle's surface.

Because of the conservative nature of the analysis performed here, the 7 dB figure is indeed an upper bound. For example, the approach taken to evaluate the radiated sound power at panel modal frequencies may have biased the result, especially for the streamwise coherence. But it is important to remember that the data evaluated in this paper was taken towards the front of the aircraft in a relatively thin boundary layer (7 cm) and may not be indicative of the sensitivities and uncertainties that exist towards the aft of larger aircraft.

It is concluded that the current gap between boundary layer model predictions and observed behavior is too large to support accurate predictions of panel response and related acoustic radiation. Designing to worst case will result in overbuilt structure, additional acoustic treatment, and, in the case of launch vehicles, reinforced payloads. A reduction in the uncertainty in boundary layer predictions would yield more efficient aerospace vehicles. This may be achieved through additional investment in acquiring the source and response data necessary to completely characterize the boundary layer over a vehicle's surface.

VIII. References

[1]M. K. Bull, Wall-pressure fluctuations beneath turbulent boundary layers: some reflections on forty years of research. Journal of Sound and Vibration (1996), 190(3), pp. 299-315.

[2]W. R. Graham, A comparison of models for the wavenumber frequency spectrum of turbulent boundary layer pressures. Journal of Sound and Vibration (1997), 206(4), pp. 541-565.

[3]Y.F. Hwang, W. K. Bonnessa and S. A. Hambric, Comparison of semi-empirical models for turbulent boundary layer wall pressure spectra. Journal of Sound and Vibration (2009), 319(1-2), pp. 199-217.

[4]G. Corcos, The structure of the turbulent pressure field in boundary layer flows. Journal of Fluid Mechanics - Cambridge Journal Online (1964), 18, pp. 353-378.

[5]G. Corcos, Resolution of pressure in turbulence. Journal of the Acoustical Society of America (1963), 35(2), pp. 192-199.

[6]B. M. Efimtsov, Characteristics of the field of turbulent wall pressure fluctuations at large Reynolds numbers. Soviet Physics-Acoustics (1982), 28 (4), pp. 289-292.

[7]D. M. Chase, Modelling the wavevector-frequency spectrum of turbulent boundary layer wall-pressure. Journal of Sound and Vibration (1980), 70(1), pp. 29-67.

[8]D. M. Chase, The character of the turbulent wall pressure spectrum at subconvective wavenumbers and a suggested comprehensive model. Journal of Sound and Vibration (1987), 112(1), pp. 125-147.

[9]A. V. Smol'yakov and V. M. Tkachenko, Model of a field of pseudonic turbulent wall pressures and experimental data. Soviet Physics-Acoustics (1991), 37 (6), pp. 627-631.

[10]D. L. Palumbo, Measurement of the Correlation and Coherence lengths in Boundary Layer Flight Data, NASA Technical Memorandum, TM-2011-217060 (2010).

[11]Rizzi, S.A., Rackl, R.G., & Andrianov, E.V., "Flight test measurement from the TU-144LL structure/cabin noise experiment", NASA TM-2000-209858, 2000.

[12]Efimtsov, B.M, Golubev, A.Y, Kuznetsov, V.B, Rizzi, S.A., Andersson, A.O, Rackl, R.G., and Andrianov, E.V., "Effect of transducer flushness on measured surface pressure fluctuations in flight", AIAA Paper 2005-0800, Jan. 2005.

[13]Palumbo, D, "Characteristic lifelength of coherent structure in the turbulent boundary layer", *AIAA Journal*, Vol. 6. No. 4, pp. 810-823, April, 2008.

[14]J. Rocha, D. Palumbo, On the sensitivity analysis of sound power radiated by aircraft panels to turbulent boundary layer parameters, Journal of Sound and Vibration, TBD.

[15]J. da Rocha, A. Suleman and F. Lau, Prediction of flow-induced noise in transport vehicles: development and validation of a coupled structural-acoustic analytical framework, Canadian Acoustics (2009), 37 (4), pp. 13-29.

[16]C. Wallace, Radiation resistance of a rectangular panel. The Journal of the Acoustical Society of America (1972), 51(3), pp. 946-952.